Structures 72 (2025) 108211

Contents lists available at ScienceDirect

Structures

journal homepage: www.elsevier.com/locate/structures

Fragility assessment and q-behaviour factor of concentrically braced steel frames under seismic sequences based on Cloud Analysis

Marco Fasan, Riccardo Del Bello, Giovanni Smiroldo, Chiara Bedon *

Department of Engineering and Architecture, University of Trieste, Trieste, Italy

ARTICLE INFO

Keywords:
Steel frames
Concentrical braced frame (CBF)
Seismic sequences
Intensity measure (IM)
Fragility curves

ABSTRACT

The structural analysis and design of multi-story buildings subjected to seismic sequences represents a well-known intriguing research topic, which has been addressed in last decades by several studies and investigations, but still lacks of a more generalized discussion. The primary goal of this paper, in this regard, is to investigate the seismic response of multi-story steel braced frames, in order to assess more in detail their capacity demand and ductility when subjected to seismic sequences, compared to single events. To this aim, two different multi-story steel structures – characterized by the use of concentrically braced frame (CBF) solutions based on cross-X with active tension diagonals (STR1) or inverted V (Chevron) bracings (STR2) respectively – are preliminary designed according to standards and examined for seismic fragility considerations. Their performance assessment is carried out using unscaled real ground motion records and employing a total of 190 non-linear dynamic simulations (95 for each building), within the Cloud Analysis framework. Different intensity measures (IMs) are considered to evaluate the impact of structural features and details on the seismic performance of STR1 and STR2 systems, namely on the associated fragility, ductility and dissipation capacity parameters. Fragility curves are in fact derived for the examined structures, based on conventional linear regression models and lognormal distribution. The corresponding *q*-behaviour factor is also calculated, by accounting for several influencing parameters. From the critical discussion of parametric numerical results, as shown, emerges that the herein considered fragility method leads to seismic assessment outcomes that highlight the effect of seismic sequences on the examined structural typology, compared to main-shock or first-shock seismic events. Most importantly, the corresponding *q*-factor is also affected by seismic sequences. The presented approach and results, in conclusion, can offer a robust support towards the definition and/or refinement of specific design recommendations, as well as and practical approaches for structural design applications.

1. Introduction

As known, the dynamic and seismic behaviour of building and infrastructures is a complex issue that is significantly affected by many influencing parameters. These parameters typically include some basic structural features (such as the in-plan and in-height regularity, the structural typology, the constructional material, etc.), the seismic input features (namely a single seismic event or a full seismic sequence) and the assessment / analysis method. For steel structures and buildings, special attention is required for dissipative mechanisms, hierarchy principles and connection details [1]. Multi-storey steel braced buildings necessitate of specific modelling strategies [2] and experimental analyses [3–6].

In this paper, the attention is given to the seismic analysis of multi-storey concentrically braced steel buildings and to assessment of major effects due to repeated events (seismic sequences). Usually, earthquakes are in fact not associated to isolated events, but commonly followed by several after-shocks with intensity even comparable to the main-shock. As such, the structural performance and capacity of steel structures should be properly addressed [7,8]. From the practical point of view, the major issue is that current technical regulations for seismic design of structures (i.e., [9–11]) do not take into account the possible effects of the seismic sequences, which means that they are commonly designed only to resist a single event (main-shock).

In this regard, the goal of present investigation is to explore in detail the typical structural and fragility trends, and to assess a possible general methodology to account for seismic sequences in structural design, for multi-storey concentrically braced steel buildings. The herein

* Correspondence to: Via Valerio 6/1, Trieste 34127, Italy.
E-mail address: chiara.bedon@dia.units.it (C. Bedon).

https://doi.org/10.1016/j.istruc.2025.108211
Received 13 August 2024; Received in revised form 5 December 2024; Accepted 7 January 2025
Available online 16 January 2025

reported study follows and extend previous efforts, such as [12–14], and reports some major outcomes of the ongoing Italian DPC-ReLUIS research project [15].

In [12], Amadio et al., investigated the effect of seismic sequences on the response of steel moment resisting frames, based on the analysis of single-degree-of-freedom (SDOF) systems with non-linear behaviour. It was shown that repeated events can lead to a significant accumulation of damage and a consequent reduction in the ductility capacity (i.e., q-behaviour factor) of these systems. The study by Fragiacomo et al. [13] also assessed the response of SDOF systems and real steel structures under seismic sequences, including moment resisting frames with rigid joints, moment resisting frames with semi-rigid joints and concentrically braced frames. A first proposal of reduced q-factor (compared to singe event) was presented to account for cumulative damage due to seismic sequences. In [14], a single-storey industrial steel building with concentrical bracings was also explored under seismic sequences, to possibly quantify a reliable reduction for the q-factor.

As the probability of damage accumulation (and thus the fragility of the structure) increases under the effect of seismic sequences, more extended and refined studies are required to address this issue, including not only pure structural considerations, but also seismic hazard evaluations [16,17].

The analysis is carried out with the support of SeismoStruct software [18], in the framework of the Cloud Analysis Method. The examined STR1 and STR2 multi-storey steel buildings – characterized by the use of concentrically braced fame frame (CBF) solutions based on cross-X with active tension diagonals (STR1) or inverted V (Chevron) bracings (STR2) respectively – are preliminary designed according to technical standards (Section 2). The numerical modelling approach and validation is summarised in Section 3. The fragility analysis is discussed in Section 4, where major working assumptions are discussed. Comparative results are finally discussed in Section 5, in terms of fragility curves and calculated q-factors for the examined systems.

2. Case-study buildings

2.1. Design parameters

The examined structures discussed in this paper consist of two three-dimensional multi-story steel buildings with concentrically braced frame (CBF) systems. Both the buildings are characterized by an identical location of high seismicity in Italy (Tolmezzo (Udine)), where the soil features according to the Italian Building Code (NTC2018 [10]) correspond to soil category C and topographic category T1. The parameters used in the design process are summarised in the following Table 1:

According to [10], moreover, the buildings were designed as residential multi-story systems with concentric bracings and Medium Ductility Class (“CDB”), by taking into account the corresponding hierarchy criterion and associated rules.

From a structural point of view, the examined buildings were preliminary designed and verified, based on the NTC2018 provisions, as regular in plan and in elevation structures, and accounting for some fixed parameters, namely the number of floors (4), the presence of a flat roof at 14 m from ground, and the plan dimensions (18 × 18 m), see Fig. 1.

S275 steel type was considered for all the structural components. The seismic-resistant part of the examined structures, finally, was set to be composed by four concentric bracings, which were symmetrically positioned at the central spans of the perimeter frames, on each side of buildings.

The most important variation, as shown in Fig. 1, was in fact represented by the different bracing layout, which was designed as a X-CBFs solution with active tension diagonals for the herein called “STR1” building and as an inverted V (Chevron) CBFs solution for “STR2” system respectively. Accordingly, the primary and secondary steel members were also detailed and designed to satisfy the NTC2018 verifications, hence resulting in mostly different details and structural features for them. Following [10], more in detail, the preliminary seismic design was carried out considering a q-behaviour factor equal to 4 and 2 for STR1 and STR2 systems respectively, as a major effect of the different CBF solution.

Table 1
Design parameters.

STRUCTURAL STEEL						
S275	f_{yk}	E	ρ	γ_{M0}	γ_{M1}	γ_{M2}
	[N/mm^2]	[N/mm^2]	[kN/m^3]	-	-	-
	275	210000	78.5	1.05	1.10	1.25
BOLT STEEL						
8.8	F_{yb}			F_{tb}		
	[N/mm^2]			[N/mm^2]		
	649			800		
LOADS						
Building category	Residential building			A		
Variable actions	q_k		[kN/m^2]		2.00	
Snow load	q_s		[kN/m^2]		1.35	
Weight of infill walls	g_k		[kN/m]		7.83	
Floor slab weight	G1		G2 (Floor slab)		G2 (Roof)	
	[kN/m^2]		[kN/m^2]		[kN/m^2]	
	2.23		2.9		1.95	
SEISMIC LOAD						
V_R	50					
Location	Tolmezzo (UD), Italy					
Soil category	C					
Topographic category	T1					
	STR1			STR2		
Behaviour factor - q	4			2		

The floors and the flat roof were assumed as composite steel-concrete resisting sections. Additionally, they were both designed as a system of beams arranged according to a regular double grid pattern. The design loads (both permanent and accidental) were defined in accordance with [10], as for a residential destination.

By taking advantage of CBFs, the steel beams were designed to sustain vertical loads only, according to a simply supported setup (hinged ends). Based on the arrangement of floors, four different section types were finally selected (Fig. 2), consisting of Class 1, IPE or HE profiles, and considering:

- Secondary beams (T1 and T2 types): orthogonal to the floor framing, and supporting floor loads (and additional loads from the external partition walls, for T2 beams).
- Primary beams (T3 and T4 types): parallel to the floor framing, supporting the secondary beams.

Regarding the steel columns, the preliminary design was conducted considering vertical loads from the Ultimate Limit State (ULS) combination, excluding seismic effects. Subsequently, the columns were also checked against the seismic combination of design actions [10], including buckling analyses. The design and verification of bracings was developed with the support of EC3 and EC8 recommendations [9, 19].

This resulted in HE240A and HE360A columns for STR1 and HE240A and HE360B columns for STR2, see Fig. 2. Overall, for STR1, the design compressive load was estimated in an average ratio of ≈ 0.51 the design resistance of each column (with maximum and minimum values of 0.55 and 0.38 respectively). For STR2, an average ratio of ≈ 0.66 was obtained (with maximum and minimum values of 0.81 and 0.42 respectively).

Regarding the bracings, the capacity-to-demand ratio Ω for the X-CBF diagonals in tension of STR1 was calculated in the range from 1.25 to 1.07 ($\Delta\Omega$= 18 % < 25 %). The cross-section detailing resulted in a non-dimensional slenderness $\bar{\lambda}$ in the range from 1.94 to 1.78 ($1.3 \leq \bar{\lambda} \leq 2$).

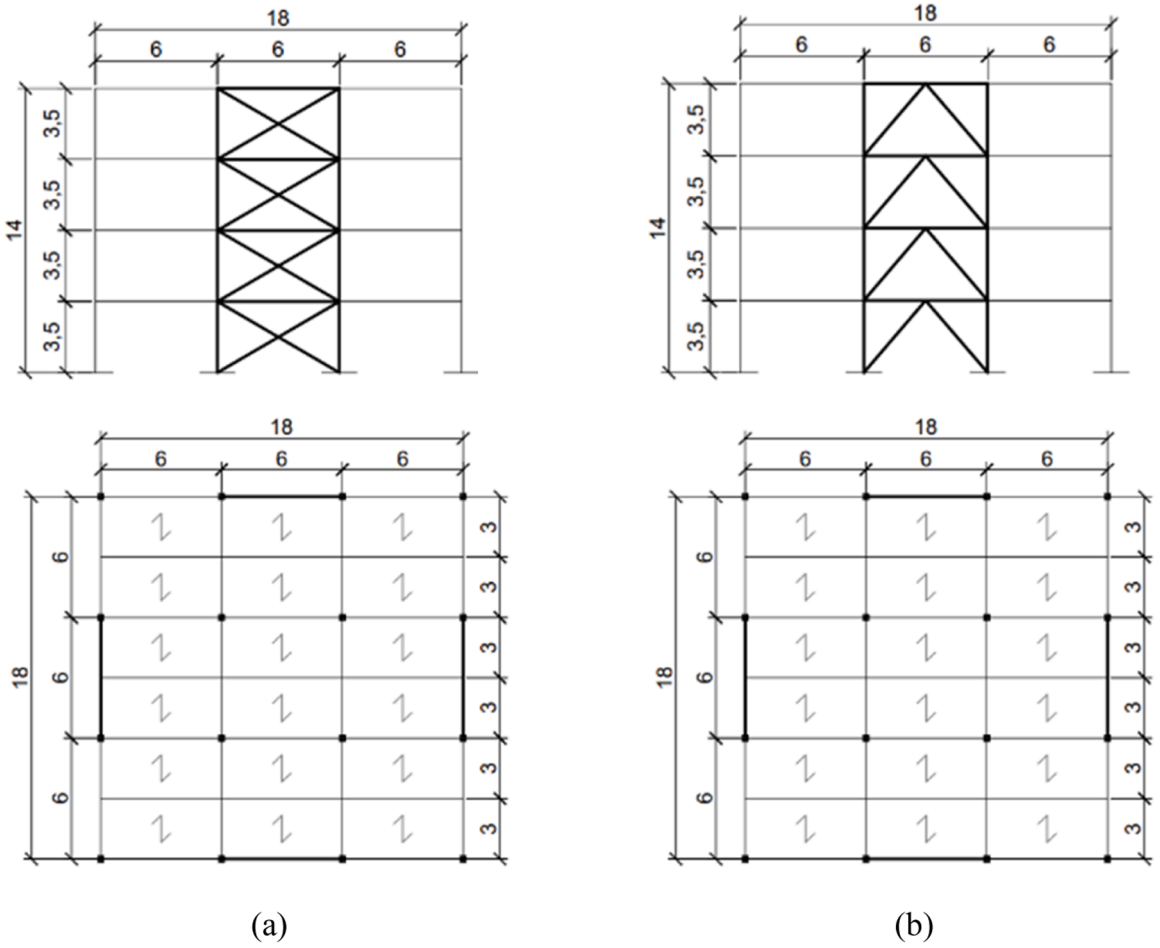

Fig. 1. Structural configuration (side and top views) for the examined (a) STR1 and (b) STR2 buildings.

For the diagonals in tension of STR2, the ratio scatter $\Delta\Omega = 22\ \% < 25\ \%$ was estimated. Regarding the diagonals in compression, the average ratio of ≈ 0.86 was calculated between the design compressive action and resistance of each member. The non-dimensional slenderness resulted in a maximum of 0.971 ($\bar{\lambda} \leq 2$). For the calculation of the non-dimensional slenderness, it is important to note that the effective length of the bracing was considered reduced, to account for the presence of the connection. The beams of STR2 system, that were also verified in bending for the seismic combination, resulted in an average ≈ 0.79 ratio between the design bending moment and the corresponding resistance. The flexural-torsional verification of the same members resulted in about a ≈ 0.82 ratio.

All the structural details (connections and joints) were also separately designed and verified for STR1 and STR2 assemblies, according to standards.

3. Structural modelling

3.1. Strategy

Each structural component for STR1 and STR2 systems was modelled using the FEM software SeismoStruct [18]. In doing so, both the beams and the columns were represented by elastic elements, while the diagonal bracing components were described with the infrmFB element of SeismoStruct library, incorporating material non-linearities through a diffused plasticity model via the use of fiber-section discretization. The cyclic uniaxial stress-strain behaviour of steel was modelled using the Menegotto-Pinto constitutive law [20].

The modelling stage included the definition of "Releases" to avoid bending moment components (see for example Fig. 3(a)), as well as a special attention for the description of structural details [21, 22], with the support of "Link" elements (Fig. 3(b)). Following [21,22] specifications, to model the behavior of the connection plate joining the braces to the beam-column node, a rotational spring is used: his is represented by a Link element, which simulates the rotation of the connection plate in a linearly elastic manner. The gusset plate is modeled using a rigid segment that connects the beam-column node to the point where the brace attaches to the plate, along with a rotational spring (modeled via the Link element) positioned at the end of the rigid segment. Each floor in the model has its own Link element, adjusted according to the section of the braces. The stiffnesses for the different degrees of freedom are determined based on the brace's stiffness, increased to meet the constraints required for the torsional and flexural behavior of the connection.

The stiffness parameters are set as follows:

- For translational degrees of freedom (F1, F2, F3), stiffness is set equal to the axial stiffness of the corresponding brace section, increased by 100 times.
- For the torsional response of the spring (M1), stiffness is set equal to the torsional stiffness of the corresponding brace section, increased by 10 times.
- For the out-of-plane flexural response of the spring (M2), stiffness is set equal to the out-of-plane flexural stiffness of the corresponding brace section, increased by 10 times.
- For the in-plane flexural response of the spring (M3), stiffness is set equal to the in-plane flexural stiffness of the corresponding brace section, increased by 10 times.

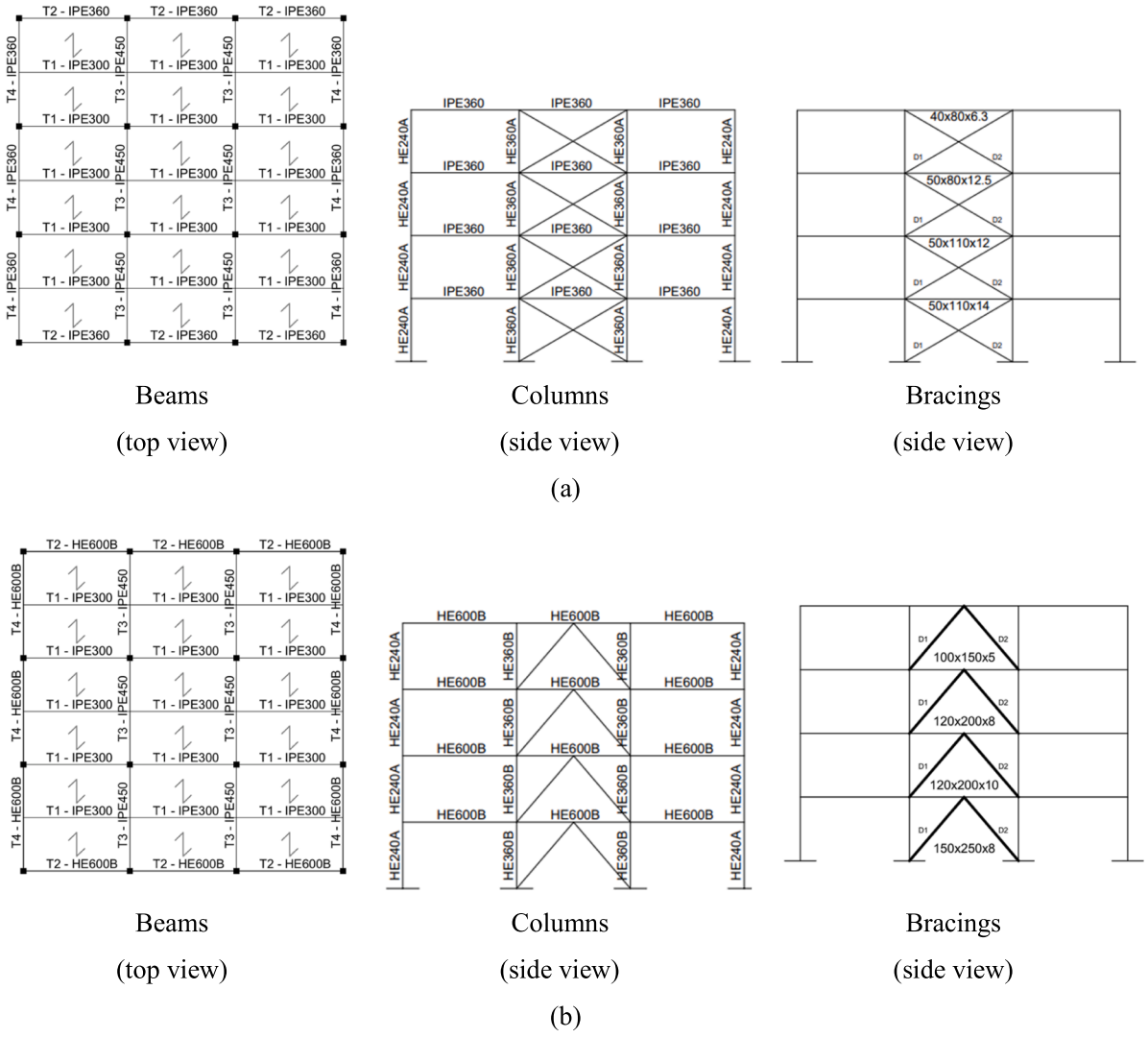

Fig. 2. Structural detailing and resisting cross-sections for the examined (a) STR1 and (b) STR2 buildings.

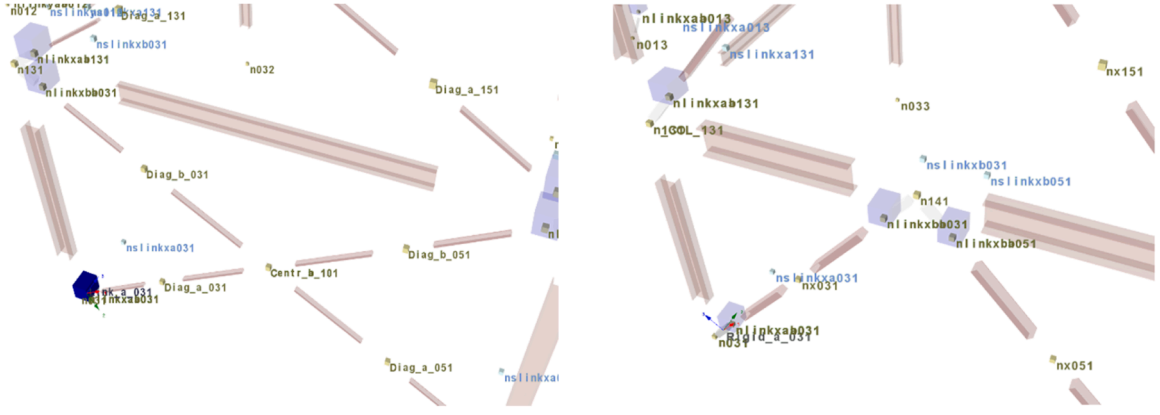

Fig. 3. Example of (a) release or (b) link details for STR1 and STR2 models.

Moreover, an initial geometrical imperfection (1/250 the maximum amplitude) was also taken into account for the bracings, according to [2, 19]. The buckling of the diagonals occurs in-plane (by design)

Fig. 4 shows the axonometric view of the final STR1 and STR2 assemblies.

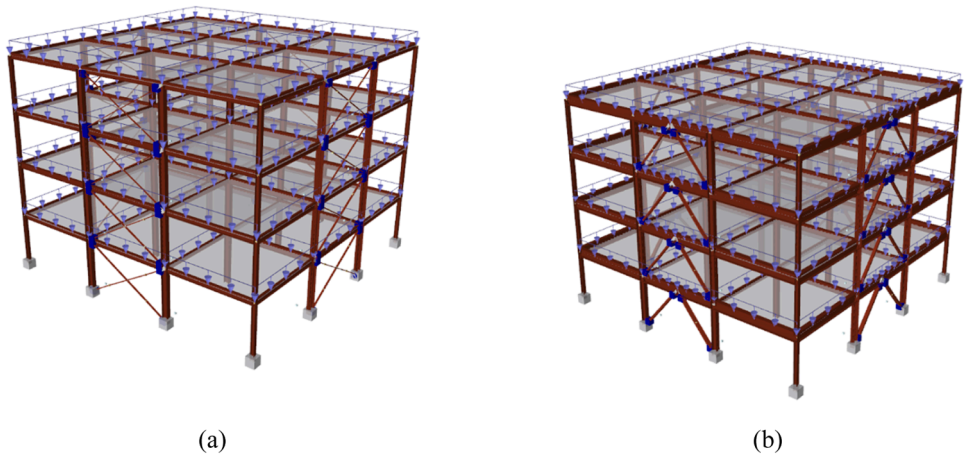

(a) (b)

Fig. 4. Axonometric view of structural models for (a) STR1 and (STR2) buildings.

3.2. Validation

The herein adopted modelling strategy and calibration was adapted for the present investigation from past efforts of the research unit, see for example [14, 15], where the attention was focused on single members, two-dimensional single-storey bracings, two-dimensional multi-storey bracings, and three-dimensional multi-storey braced systems. In any case, the input assumptions were verified against a selection of experimental results from literature. As an example of model accuracy and potential, as a preliminary validation, the experimental results reported in [3, 4] were taken into account.

Fig. 5 shows a typical comparison of past experimental responses and present modelling strategy (in red), where Fig. 5(a) refers to a single-story X-CBF [3] while Fig. 5(b) reports the comparison for one of the specimens explored in [4]. For both the selected examples, it is possible to note a rather good correlation between past experimental and present numerical estimates, and thus to confirm the validity of input assumptions.

3.3. Preliminary assessment

To further assess the overall behaviour of the assembled structural models, two types of analyses were preliminary carried out: a modal analysis to assess the structural vibrational modes, and Push-Over analysis to verify their non-linear behaviour. Additionally, verifications were performed to ensure that the seismic mass calculated by the software was in good correlation with the value obtained from the analytical structural design.

The periods and percentage of participating mass for the first three vibrational modes are summarized in Table 1. As expected, the first two modes are translational in the longitudinal and transversal directions, while the third represents the torsional one (Fig. 6). To note in Table 2 that the vibration period is markedly different, due to the major variation in CBFs design and in the consequent detailing of primary and secondary steel members.

The Push-Over analysis for STR1 and STR2 assemblies was carried out accounting for triangular / first-mode proportional (D1) and uniform distribution of lateral loads (D2). As a confirmation of modelling consistency, the percentage scatter for the calculated seismic masses of STR1 and STR2 assemblies was estimated in less than 1 %, see Table 3.

Finally, to check further the modelling accuracy, the theoretical critical buckling load $N_{b,Rd}$ was calculated according to [10], and verified towards the corresponding numerical estimates, based on Push-Over analyses. Table 4 presents the comparative results, confirming a rather good consistency.

4. Fragility analysis

The selection of seismic records, as known, represents a critical step for fragility analysis and considerations [23–25]. The corresponding fragility curves, which are typically developed using non-linear time--history analyses, could reveal some sensitivity [26]. In support of the present investigation, the Cloud Analysis procedure was chosen, due to its relatively low computational cost [15, 27, 28]. Moreover, it relies on the use of unscaled ground motion records, thereby reducing potential biases introduced by scaling [29–33].

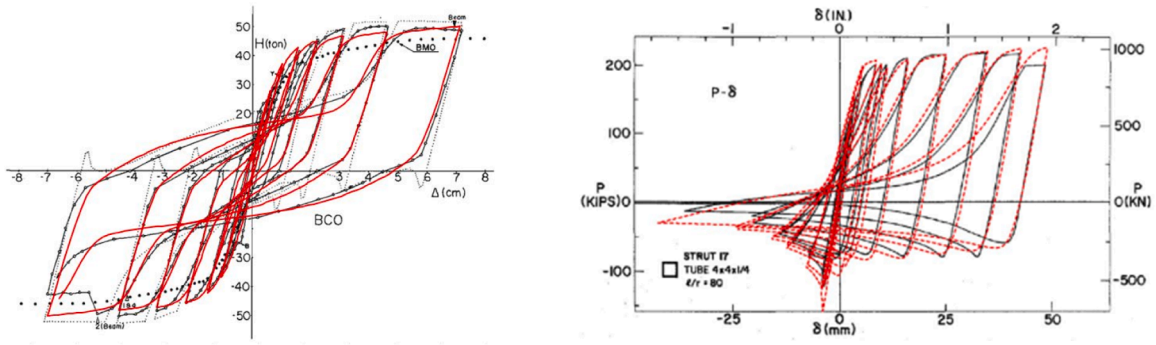

(a) (b)

Fig. 5. Model validation towards past experimental results (adapted from [3, 4]).

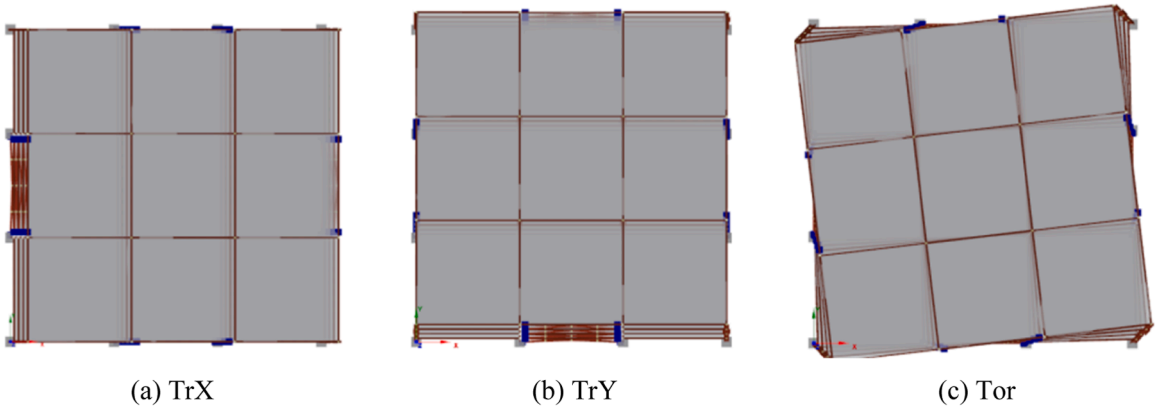

Fig. 6. Fundamental vibration shapes (top view) for STR1 and STR2 buildings.

Table 2
Vibration periods and percentage participating mass for the lower modes of the examined structures. Key: TrX= translational in the *x*-direction; TrY= in the *y*-direction; Tor= torsional.

	STR1			STR2		
Mode	**Type**	**Period [*s*]**	**Participating mass [%]**	**Type**	**Period [*s*]**	**Participating mass [%]**
		T_i	M_i		T_i	M_i
1	TrX	0.5805	79.94	TrX	0.4424	78.44
2	TrY	0.5804	79.87	TrY	0.4423	78.51
3	Tor	0.3856	79.49	Tor	0.2960	77.80

Table 3
Weight of seismic masses.

STR1			STR2		
Analytical [kN]	**Numerical [kN]**	**Δ [%]**	**Analytical [kN]**	**Numerical [kN]**	**Δ [%]**
8944.81	8900.08	0.503	9351.16	9287.33	0.687

4.1. Earthquake record selection

For the present investigation, real ground motion records were selected from the ESM and Strong-Motion Seismograph Networks databases [34,35], which collect accelerograms of seismic events in Europe/Middle East and Japan, respectively. For each seismic sequence, the main-shock (i.e., the event with maximum Peak Ground Acceleration in the sequence) and the first-shock were identified. Subsequently, the seismic signals representing the entire sequences were created by arranging events sequentially, with 30 s intervals between each shaking, and thus allowing the STR1 and STR2 buildings to stop the oscillatory motion before experiencing subsequent shaking. At the same time, the strategy allowed to account for cumulative damage.

This approach resulted in three groups of input acceleration time-histories, each one including 35 accelerograms, for the non-linear dynamic analyses. Table 4 lists the selected seismic records, where the first letter of each signal identifies the seismic event, while the acronym defines the station where the event was recorded (F=Friuli 1976; NU=Nocera Umbra 1977; E = Emilia-Romagna 2012; M=Molise 2002; J=Japan 2004/2008/2010/2011; N = Central Italy 2016).

For clarity needs, Table 5 shows the list of the selected Mainshock ground motions records only, while Table 6 shows the list of selected seismic sequence events and recording stations.

As an example, Fig. 7 displays the accelerogram of the seismic sequence of the 1976 Friuli earthquake recorded at the Gemona station (GMN) in the North-South component. Overall, a total of 190 non-linear dynamic analyses was carried out (95 for STR1 and 95 for STR2 buildings), accounting for 35 main-shocks, 25 first-shocks and 35 full seismic sequences for each structural model.

Additionally, the spectra of both first-shock and whole sequence of Friuli (1976), recorded by the Gemona Station (GMN) is illustrated in the following Fig. 8:

4.2. Intensity measure selection

For each time-history of the three groups described in Section 4.1., three different Intensity Measures (IM) were considered as suggested in [36], and namely included:

- PGA= Peak Ground Acceleration,
- $S_a(T_{1m})$ = average spectral acceleration of the first two translational modes:

$$S_a(T_{1m}) = S_a\left(\frac{T_{1x} + T_{1y}}{2}\right) \quad (1)$$

Table 4
Critical buckling loads for bracings.

	STR1				STR2			
Floor	**Profile**	**Analytical [kN]**	**Numerical [kN]**	**Δ [%]**	**Profile**	**Analytical [kN]**	**Numerical [kN]**	**Δ [%]**
P4	40 × 80 × 6.3	116.90	132.87	−12.0	100 × 150 × 5	415.64	529.06	−21.4
P3	50 × 80 × 12.5	250.99	300.34	−16.4	120 × 200 × 8	974.79	1121.71	−13.1
P2	50 × 110 × 12	348.74	391.97	−11.0	120 × 200 × 10	1182.13	1378.34	−14.2
P1	50 × 110 × 14	360.55	394.07	−8.5	150 × 250 × 8	1379.94	1498.13	−7.9

Table 5
List of selected Mainshocks ground motion events.

ID	Event ID	Event name	Station code	Magnitude Mw	Focal mechanism	Soil category	Epicentral distance [km]	PGA [cm/s^2]
1	IT−1976–0025	Friuli	BUI	5.6	TF	C	11.7	168
2	IT−1976–0030	Friuli	FRC	6	TF	B	16.2	334
3	IT−1976–0030	Friuli	SRC0	6	TF	B	15.8	178
4	IT−1997–0006	Nocera Umbra	ASS	6	NF	B	21.6	161
5	IT−1997–0004	Nocera Umbra	CLF	5.7	NF	D	2.8	289
6	IT−1997–0137	Nocera Umbra	FHC	5.6	NF	A	29.5	62
7	IT−1997–0006	Nocera Umbra	GBP	6	NF	C	38.4	96
8	IT−2002–0045	Molise	GLD	5.7	SS	B	25.2	13
9	IT−2012–0008	Emilia-Romagna	MRN	6.1	TF	C	16.1	286
10	IT−1997–0006	Nocera Umbra	NCR	6	NF	E	10.9	522
11	IT−2012–0011	Emilia-Romagna	NVL	6	TF	C	26.4	50
12	IT−2012–0008	Emilia-Romagna	SRP	6.1	TF	C	64.7	30
13	IT−2002–0045	Molise	SSV	5.7	SS	B	38.1	52
14	IT−1976–0002	Friuli	TLM1	6.4	TF	B	27.7	312
15	IT−2002–0045	Molise	VSE	5.7	SS	B	50.8	27
16	IT−1976–0027	Friuli	GMN	5.9	TF	B	6.2	459
17			NIG017	6.8				477
18			NIG019	6.8				290
19			NIG021	6.8				141
20			MYG004	7.2				403
21			FKS006	5.5				715
22			FKS001	7.1				426
23			FKS003	9				1237
24			IBR003	7				1462
25			IBR003	5.3				228
26	EMSC−20161030_0000029	Norcia	AMT	6.5	NF	B	26.4	507
27	EMSC−20161030_0000029	Norcia	AQG	6.5	NF	B	54.2	62
28	EMSC−20161030_0000029	Norcia	ASP	6.5	NF	C	44	115
29	EMSC−20161030_0000029	Norcia	CSC	6.5	NF	B	14.9	157
30	EMSC−20161030_0000029	Norcia	GBP	6.5	NF	C	68.3	51
31	EMSC−20161030_0000029	Norcia	GNU	6.5	NF	A	44.3	38
32	EMSC−20161030_0000029	Norcia	MNF	6.5	NF	A	26	119
33	EMSC−20161030_0000029	Norcia	NOR	6.5	NF	B	4.7	330
34	EMSC−20161030_0000029	Norcia	NRC	6.5	NF	B	4.6	375
35	EMSC−20161030_0000029	Norcia	SPD	6.5	NF	B*	41.2	87
36	EMSC−20161030_0000029	Norcia	SPM	6.5	NF	A	31.8	85
37	EMSC−20161030_0000029	Norcia	TRE	6.5	NF	C	31	114

Table 6
List of selected seismic sequences events and stations.

F.BUI	NU.ASS	E.MRN	M.SSV	J.FKS001	N.AMT
F.FRC	NU.CLF	E.NVL		J.FKS003	N.AQG
F.SRC0	NU.FHC	E.SRP		J.FKS006	N.ASP
F.TLM1	NU.GBP			J.IBR003	N.CSC
F.GMN	NU.NCR			J.MYG004	N.GBP
				J.NIG017	N.GNU
				J.NIG019	N.MNF
				J.NIG021	N.NOR
				J.IBR0032	N.NRC
					N.SPD
					N.SPM
					N.TRE

- $S_{a,avg}(T_i)$ = average spectral acceleration defined as the geometric mean of the spectral accelerations over a range of periods:

$$S_{a,avg}(T_i) = \left[\prod_{i=1}^{n} S_a(T_i)\right]^{1/n} \tag{2}$$

where T_i represents the following periods:

$$T_i = \left[T_{2m}, \min\left[\frac{T_{2m}+T_{1m}}{2}, \quad 1.5 \bullet T_{2m}\right], \quad T_{1m}, \quad 1.5 \bullet T_{1m}, \quad 2 \bullet T_{1m}\right] \tag{3}$$

All the above IMs were represented using the GMRotD50 component, representing the fiftieth percentile (D50) of the geometric mean (GM) over all possible non redundant rotation angles (Rot), see [37].

4.3. Engineering demand parameter (EDP) selection

To monitor both structural and non-structural damage, the inter-story drift ratio (IDR) is commonly chosen as most significant parameter, or Engineering Demand Parameter (EDP).

Accordingly, the inter-storey drift time-history at the *i*-th floor in direction *j* can be defined as:

$$IDR_{i,j}(t) = \frac{\delta_{ij}(t) - \delta_{i-1\,j}(t)}{h_i} \tag{4}$$

where $\delta_{ij}(t)$ is the displacement at floor *i* in direction *j* at the time instant *t*, and h_i is the inter-storey height.

For the present investigation, non-linear dynamic analyses were conducted by simultaneously applying both the horizontal components of seismic excitation. To use a unique directionless value, the maximum

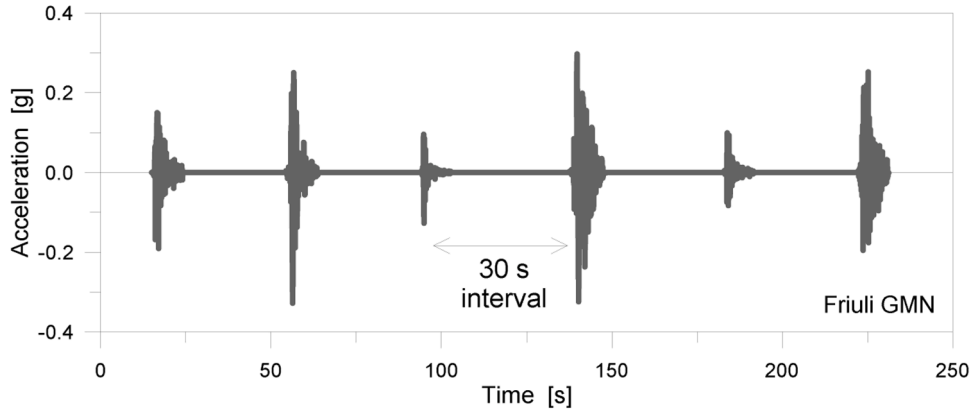

Fig. 7. Example of accelerogram for the Friuli seismic sequence (1976) recorded by the Gemona station (GMN), North-South component.

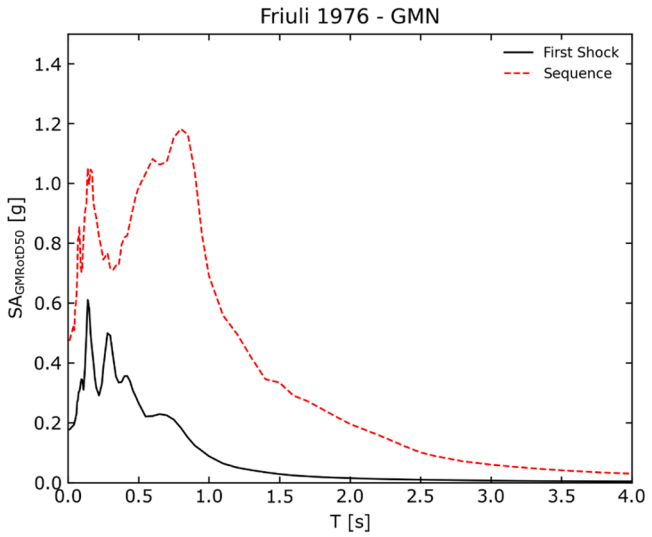

Fig. 8. Friuli seismic sequence (1976) recorded by the Gemona station (GMN) spectra for First Shock and whole sequence.

(resultant) inter-storey drift at storey i was considered as the peak (in time) of the Square Root of the Sum of Squares (SRSS) of the IDR, in the two main orthogonal directions, namely:

$$MIDR_i = \max\left(\sqrt{IDR_{i,x}^2(t) + IDR_{i,y}^2(t)}\right) \quad (5)$$

Finally, the so-defined maximum inter-story drift (MIRD) calculated for the examined buildings under an assigned seismic input was adopted as a single EDP, in order to define the level of damage reached in the structure [36]:

$$MIDR = \max(MIDR_1, \quad \ldots \quad , \quad MIDR_n) \quad (6)$$

To develop fragility curves of STR1 and STR2 systems, damage thresholds were first established. The EC8 recommendations were considered for determining the damage thresholds (EDP_{pl}) at every Limit State of interest, namely for slight damage (DL), significant damage (SD), and near collapse (NC). Most importantly, the EC8 was taken into account to define the capacity limits for steel frames and components of STR1 and STR2 systems, including beams, columns, and tension or compression braces. For braces in tension and compression, the inelastic deformation capacity can be usually expressed in terms of axial deformation of the brace.

Table 7 summarises the relevant assumptions for the present investigation, based on EC8 (Tables B.2 and B.3), where Δ_t, and Δ_c are the axial deformation at tensile yielding or compressive buckling load respectively. The reported limit values of axial deformations for the diagonal members of bracings were further expressed in terms of the corresponding inter-story drift ratios (IDR), so as to identify the EDP values of damage thresholds, for the respective Limit States.

Table 7
Reference values of axial deformation capacity for braces in tension or compression (Class 1 cross-sections).

	Limit State		
	DL	**SD**	**NC**
Tension	0.25 Δ_t	7 Δ_t	9 Δ_t
Compression	0.25 Δ_c	4 Δ_c	6 Δ_c

4.4. Fragility functions

The fragility function for a given performance level can be conventionally defined as [29, 38]:

$$P(EDP > EDP_{pl}|IM) \quad (7)$$

Eq.(7) indicates the probability of experiencing an EDP greater than the threshold value (EDP_{pl}), given a certain value of IM. This function can be computed using the standard approach of Cloud Analysis, that supposes a linear relation between the logarithm of EDP and the logarithm of IM:

$$\ln(EDP|IM) = a + b \bullet \ln(IM) \quad (8)$$

In Eq. (8), $\ln(EDP|IM)$ represents the median estimate of the EDP given an IM value, while a and b denote respectively the intercept on the y-axis and the slope of the regression line in logarithmic scale, which is evaluated applying the Ordinary Least Square (OLS) method [36]. According to the method assumption, the residuals around the mean value are normally distributed with zero mean and constant logarithmic standard deviation, that is:

$$\sigma_{\ln(EDP)|\ln(IM)} = \sqrt{\left(\frac{\sum_n^1 (\ln(EDP_i) - \ln(EDP_i|IM_i))^2}{N-2}\right)} \quad (9)$$

with N denoting the total number of records. Therefore, given a threshold value of EDP (EDP_{pl}), the probability of experiencing an EDP greater than EDP_{pl}, given an IM value, follows a log-normal distribution and is defined as:

$$P(EDP > EDP_{pl}|IM) = 1 - \Phi\left(\frac{\ln(EDP_{pl}) - \ln(EDP|IM)}{\sigma_{\ln(EDP)|\ln(IM)}}\right) \quad (10)$$

where Φ represents the standard normal cumulative distribution function.

Fragility functions must be developed to account for the impact of uncertainties, as detailed in [39–41]. These uncertainties include various aspects such as: (i) record-to-record variability; (ii) variability in mechanical properties; (iii) variability of performance level capacity thresholds; (iv) uncertainties in model parameters. The first three can mainly be classified as mainly aleatory uncertainties, while the last one primarily concerns epistemic uncertainty. Uncertainties in statistical model parameters are accounted for using a bootstrap procedure as described in [38]. This procedure is based on the resampling with replacement of the initial input data, which leads to n different realizations and consequently to n fragility curves and n regressions. The number of bootstraps for the present study was set in 1000.

5. Results and discussion

5.1. Fragility curves

Typical results from fragility analysis of STR1 and STR2 assemblies are presented in Fig. 9, in terms of linear regression of correlations and corresponding fragility curves. For convenience, the selected figures are exemplificative results of correlations obtained for main-shocks, related to the PSA_{avg} intensity measure, followed by the corresponding fragility curves.

More in detail, in Fig. 9(a) and (b), the light grey lines represent individual realizations of the resampling procedure, while the mean plus and minus one standard deviation are depicted by solid and dashed black lines respectively. Similarly, for Fig. 9(c) and (d), the grey fragility curves represent individual realizations of the bootstrap procedure, while the average fragility curve and the 14th and 86th percentiles (plus or minus one standard deviation) are represented by solid and dashed black lines, respectively.

In general, the collected fragility curves gave evidence of some relevant modifications or even mostly negligible effects for the assigned seismic input. In some cases, the fragility analysis didn't highlight marked variations for a given structure subjected to seismic sequence of single event. In some others, the effect of seismic sequences was typically associated to higher fragility. Fig. 10 (a), for instance, shows the median fragility curves for STR1 building with X-CBFs under main-shock, first-shock or seismic sequence. There is a minimum sensitivity of fragility curves due to main-shock or seismic sequence, while a lower fragility is associated to the curve for first-shock. Fig. 10 (b) shows the fragility curves for the STR2 building with inverted V-bracings, in which a differing sensitivity in the fragility curves and expected ductility were observed, depending on the assigned seismic input. As such, the detailed analysis was further exploited in terms of q-behaviour factor trends.

5.2. q-behaviour factor

The structural factor (or *q-factor*) is commonly calculated as the ratio between the input acceleration that leads to the yielding (i.e. the acceleration that leads to the exceedance of the elastic field) and the input acceleration that leads to collapse [9, 10], giving a measure of the ductility of the structures.

Following EC8, the seismic design of buildings is conducted using the force-based design method, and the design base shear is strictly dependent on the q-factor.

In the present study, the q-factor estimation – which conventionally simplifies the quantification of complex energy dissipation capacities –

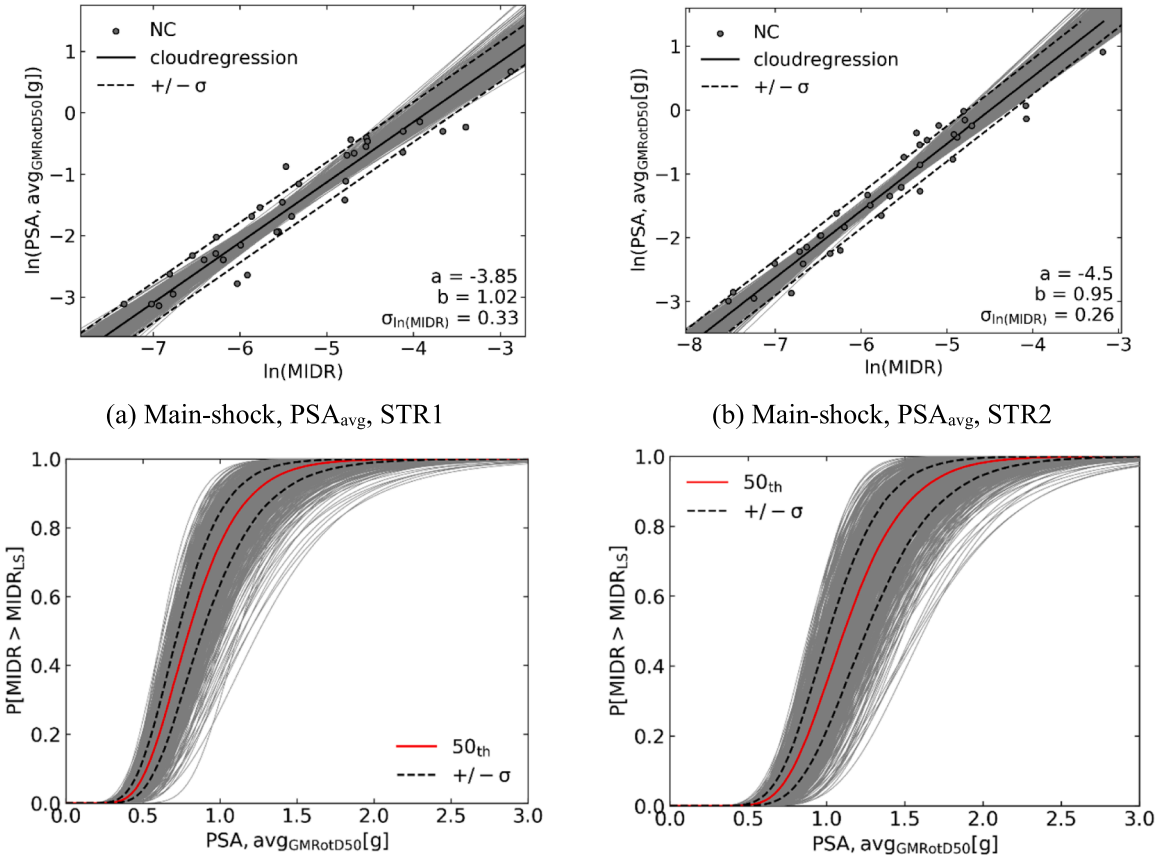

(a) Main-shock, PSA_{avg}, STR1

(b) Main-shock, PSA_{avg}, STR2

(c) Main-shock, PSA_{avg}, STR1

(d) Main-shock, PSA_{avg}, STR2

Fig. 9. Fragility analysis (selected example): (a)-(b) linear regressions and (c)-(d) fragility curves for STR1 and STR2 buildings.

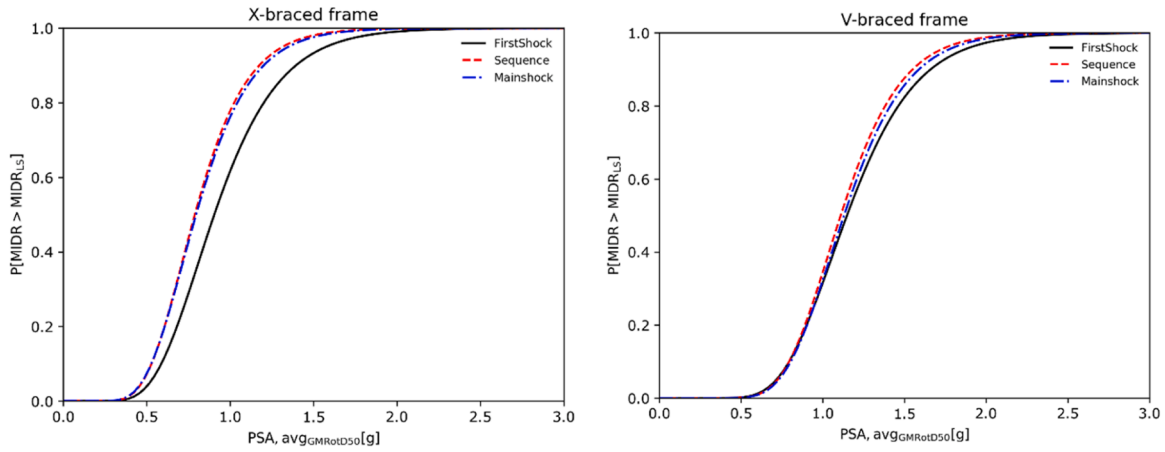

(a) X-braced frame (STR1) fragilities (b) V-braced frame (STR2) fragilities

Fig. 10. Fragility curves comparison for (a) STR1 building and (b) STR2 building.

was specifically carried out to monitor the possible effect of seismic sequences on the examined steel buildings, by using the Claud Analysis method. The loss of ductility due to single events (main-shock or first-shock) or entire sequences was thus investigated for STR1 and STR2 buildings.

5.2.1. Push-Over analysis

For comparative purposes, the q-factor was preliminary evaluated also through Push-Over analyses, as it can be easily derived based on Newmark's assumptions, namely:

$$q = \mu \text{ for} T \geq T_C \tag{11}$$

$$q = \sqrt{2\mu - 1} for T < T_C \tag{12}$$

with:

$$\mu = \frac{\delta_u}{\delta_y} \tag{13}$$

where δ_y and δ_u are the control node displacements corresponding to the time instant of non-linear dynamic analysis where the axial deformation of "first yielding" (y) and "collapse" (u) respectively are first reached for one of the diagonals.

Fig. 11 shows the results of Push-Over simulations, giving evidence of the control points corresponding to key performance indicators for STR1 (3DX) and STR2 (3DV) systems, by applying a triangular (D1) or uniform (D2) load distribution. For the investigated systems, it is possible to perceive a mostly different behaviour and base shear-lateral displacement, in terms of initial stiffness, overall strength, and ductility. Table 8 summarises the corresponding calculation of the q-factor, which is affected by all these aspects.

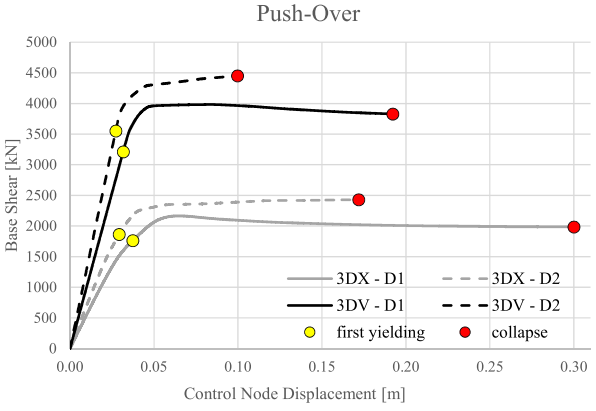

Fig. 11. Identification of key configurations corresponding to "first yielding" and "collapse" for STR1 and STR2 buildings, based on Push-Over analysis.

As shown in Fig. 11 and Table 8, there is a significant variation between the behaviour of STR1 and STR2 buildings, both for the imposed distribution of loads and for the CBFs solution. Specifically, unlike the X-bracing, the Chevron bracing is characterized by a well-known initial capacity to resist the horizontal forces that derives from the contribution of compressed diagonals. However, as illustrated in Fig. 12, their possible buckling collapse and the consequent redistribution of forces in the load-bearing components should be properly accounted for. Most importantly, the effect of different seismic input should be addressed more in detail.

5.2.2. Cloud Analysis

For more extended comparative considerations, the q-factor estimation was successively performed by using the method previously adopted in [15, 27, 28], which is based on the definition of spectral acceleration and assumes:

$$q = \frac{S_a(T_1)_u}{S_a(T_1)_y} \tag{14}$$

where $S_a(T_1)$ is the spectral acceleration corresponding to the axial deformation of the bracing diagonals in tension at yielding (y) or collapse (u), based on the limit values from EC8 at the NC condition. Table 9 summarizes the calculation of limit deformations and the corresponding IDRs. Notably, the thresholds in Table 9 associated to "collapse" are consistent with the inter-story drifts experimentally obtained in [5, 6]. Moreover, given the nature of the bracing system of STR2, in this case the "first yielding" threshold is set equal to buckling collapse of the diagonal, being representative of a first major modification of the load-bearing capacity and seismic response for the system.

Table 8
Calculated q-behaviour factor for the examined STR1 and STR2 buildings, based on Push-Over analysis.

	STR1		STR2	
	D1	D2	D1	D2
δ_y	0.03732	0.02924	0.03166	0.02724
δ_u	0.30004	0.17188	0.19216	0.09972
q	8.04	5.88	3.34	2.51

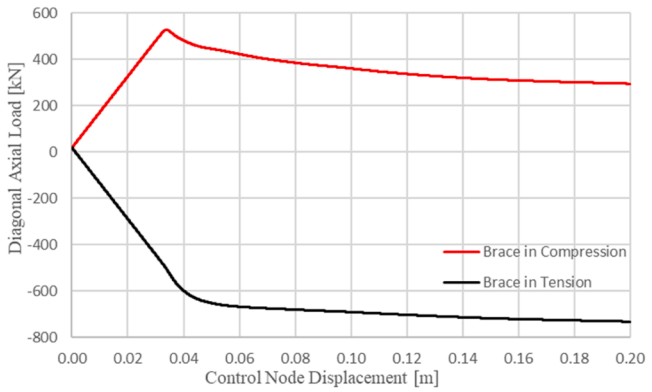

Fig. 12. Axial load trend in compressed and tensioned diagonals during Push-Over analysis for STR2.

Table 9
Thresholds for "first yielding" and "collapse" configurations (diagonals in tension).

	STR1			STR2		
	Δ_t [%]	δ [m]	IDR	Δ_t [%]	δ [m]	IDR
First yielding (y)	0.1247	0.0097	0.0028	0.1247	0.0080	0.0023
Collapse (u)	1.1224	0.0754	0.0215	1.1224	0.0548	0.0157

Accordingly, the "collapse" configuration for the active compressed diagonals was set as in Table 7.

By taking advantage of the linear regressions obtained through the Cloud Analysis method for the PSA-IDR pairs and the identified thresholds, the spectral accelerations for "first yielding" and "collapse" were finally calculated as:

$$IM_y = e^{[(\ln(EDP_y)-a)/b]} \quad (15)$$

$$IM_u = e^{[(\ln(EDP_u)-a)/b]} \quad (16)$$

In Eqs. (15)-(16), a and b are the regression parameters; EDP_y and EDP_u are the threshold in terms of IDR; IM_y and IM_u are the intensity measures, specifically the spectral accelerations.

Fig. 13 shows a typical example (related to the first-shock for STR1) for deriving the IMs from linear regressions in the bi-logarithmic field, by using the thresholds in terms of EDP (which are represented by the vertical lines). Following Section 4.2, the comparative calculation was

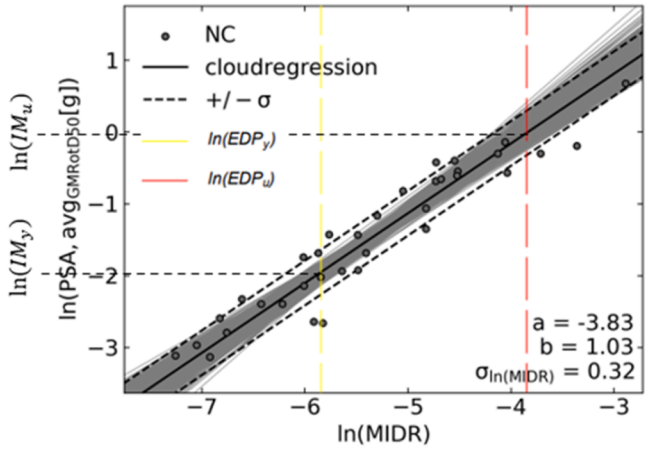

Fig. 13. Graphical identification of thresholds in terms of EDP and derivation of IMs for "first yielding" (y) and "collapse" (u) configurations (example for STR1).

carried out considering three different IMs. In Table 10, accordingly, the so-estimated q-factors are proposed for STR1 and STR1 buildings, grouped by type of event (MS = main-shock, FS = first-shock, SS = full seismic sequence) and intensity measures.

The comparative results of Table 10 in terms of q-factor emphasise some important outcomes that should be further addressed. First, there is a marked sensitivity of the estimated ductility capacity to the selected IM, which is a parameter of paramount importance for seismic design and structural safety purposes.

For the STR1 building, regardless the selected IM, the q-factor associated to the full seismic sequences (SS) is generally lower than main-shock (MS) and even lower than first-shock (FS). Such an outcome denotes the effects of cumulative damage, which is typical for seismic sequences, and should be properly taken into account. For the STR2 system, similar trends were in general observed for the system under seismic sequences, which was found associated to lowest q-factors. Most importantly, the active compressed diagonals and their buckling collapse have major consequences on the overall seismic response and ductility capacity, as it can be perceived from the comparative values of Table 10. Notably, as far as the key performance indicators are considered for STR2 on the diagonals in tension only, the associated ductility capacity is markedly higher and mostly in line with STR1. Again, moreover, the lowest q-factor values are still associated to the building under seismic sequences, rather than single events.

Such an effect is particularly important, and was only partly emphasised by fragility curves. Overall, as expected, the comparative analyses suggested that there are some important effects due to input seismic sequences, that should be properly considered for design. In this sense, further extended studies will be carried out on different datasets of input signals, as well as on different structural models and typologies, in order to derive more robust and generalized recommendations.

6. Conclusions

Seismic sequences, as known, can involve important effects on structures and should be properly taken into account for design and retrofit. Besides, technical standards currently disregard this aspect, and structural systems are conventionally designed against a single event.

In order to collect some useful recommendations, the main objective of present study was to investigate the effects of seismic sequences on multi-story steel frames with concentric of bracing, assessing their fragility and estimating the corresponding q-behaviour factor by using the Cloud Analysis procedure.

To this aim, two different multi-story structures – characterized by the use of concentrically braced frame (CBF) solutions based on cross-X with active tension diagonals (STR1) or inverted V (Chevron) bracings (STR2) respectively – were preliminary designed according to standards. The seismic performance assessment, carried out in the form of 190 non-linear dynamic simulations (95 for each building), posed the attention on the effects of cumulative damage, as well as on different intensity measures (IMs), which were considered to evaluate the associated fragility, ductility and dissipation capacity parameters.

Based on the collected numerical results, while disregarding a direct comparative analysis of STR1 and STR2 performances, it was possible to observe some important outcomes. More in detail, the analysis of the developed fragility curves was not univocally associated to increased fragility, for STR1 or STR2 buildings subjected to seismic sequences. In terms of q-behaviour factor, the calculated values in presence of seismic sequences typically revealed an increase in fragility (corresponding to a loss of ductility), when considering the STR1 and STR2 systems subjected to full seismic sequences or main-shocks respectively. The results show that for STR1, such a fragility increase in presence of seismic sequences was reduced to a minimum, compared to main-shocks, whilst for STR2, the results show a minimum difference between all three different seismic input. As such, the possible recommendation of a reduced q-factor for accounting for repeated seismic events, in this

Table 10
Calculated q-behaviour factor for the examined STR1 and STR2 buildings, based on Cloud Analysis.

	STR1			STR2Active compressed diagonals			STR2		
IM	MS	FS	SS	MS	FS	SS	MS	FS	SS
PGA	7.77	9.07	7.77	1.65	1.65	1.64	7.56	7.72	7.25
PSA_{T1m}	9.29	10.01	9.07	1.68	1.66	1.65	8.07	7.89	7.56
PSA_{avg}	7.46	8.46	7.32	1.65	1.64	1.62	7.56	7.56	7.10

sense, is in line and reconfirms past proposals of literature. Besides, such an increase of fragility – and thus the corresponding reduction of q-factor – still requires further extended investigation, before a general proposal could be developed. For instance, since cumulative rotation capacities are not specified within seismic codes, the numerical model would need to incorporate the low-cycle fatigue metric to more accurately account for the effects of cumulative damage.

The presented approach and results, in conclusion, proved to offer a robust support towards the definition and refinement of specific design recommendations for structures subjected to repeated seismic events. Further studies will be carried out in support and extension of present results.

CRediT authorship contribution statement

Marco Fasan: Writing – original draft, Software, Methodology, Conceptualization. **Riccardo Del Bello:** Writing – original draft, Visualization, Investigation, Formal analysis, Data curation. **Giovanni Smiroldo:** Writing – original draft, Software, Formal analysis, Data curation. **Chiara Bedon:** Writing – original draft, Supervision, Resources, Funding acquisition.

Declaration of Competing Interest

The authors declare there is no conflict of interest with the publication of present research study.

Acknowledgements

DPC-ReLUIS is gratefully acknowledged for facilitating, in the years, a fruitful scientific networking of the involved authors with several esteemed experts, and for providing financial support to the team members of University of Trieste research unit. This research article is dedicated to the memory of our respected mentor and colleague Prof. Claudio Amadio.

References

[1] Landolfo R, Mazzolani F, Dubina D, da Silva LS, D'Aniello M. Design of STeel Structures for Buildings in Seismic Areas: Eurocode 8: design of structures for earthquake resistance. Part 1-1 – general rules. Seismic Actions and Rules for Buildings. Wiley; 2017. p. 491. ISBN: 9783433030103.
[2] D'Aniello M, Ambrosino GLM, Portioli F, Landolfo R. Modelling aspects of the seismic response of steel concentric braced frames. Steel Compos Struct 2013;15(5):539–66.
[3] Wakabayashi M, Matsui C, Minami K, Mitani I. Inelastic Behavior of Full-Scale Steel Frames with and without Bracings. Bull Disaster Prev Res Inst 1974;24(216):1–23.
[4] Black RG, Wenger WAB, Popov EP. Inelastic Buckling of Steel Struts Under Cyclic Load Reversals. Technical Report Ref: UBC/EERC-80/40 (166 pages). Earthquake Engineering Research Center. Berkeley, California: University of California; 1980.
[5] Lehman DE, Roeder CW, Herman D, Johnson S, Kotulka B. Improved seismic performance of gusset plate connections. J Struct Eng 2008;134(6). https://doi.org/10.1061/(ASCE)0733-9445(2008)134:6(890).
[6] Okazaki T, Lignos DG, Hikino T, Kajiwara K. Dynamic response of a chevron concentrically braced frame. J Struct Eng 2013;139(4). https://doi.org/10.1061/(ASCE)ST.1943-541X.0000679.
[7] Hatzigeorgiou GD. Ductility demand spectra for multiple near- and far-fault earthquakes. Soil Dyn Earthq Eng 2010;30(4):170–83.
[8] Ruiz Garcia J, Negrete-Manriquez JC. Evaluation of drift demands in existing steel frames under as-recorded far-field and near-fault mainshock-aftershock seismic sequences. Eng Struct 2011;33:621–34.
[9] EN 1998-3: Eurocode 8: Design of Structures for Earthquake Resistance – Part 3: Assessment and Retrofitting of Buildings, 2005.
[10] NTC2018. Norme Tecniche Per Le Costruzioni; Design Standard for Buildings,.17 Gennaio 2018. Ministero delle Infrastrutture e dei Trasporti, Roma, Italy (in Italian).
[11] Federal Emergency Management Agency. FEMA Publication 273. NEHRP Guidelines for the seismic rehabilitation of buildings. Washington D.C: Building Seismic safety Council; 1997.
[12] Amadio C, Fragiacomo M, Rajgelj S. The effects of repeated earthquake ground motions on the non-linear response of SDOF systems. Earthq Eng Struct Dyn 2003;32:291–308.
[13] Fragiacomo M, Amadio C, Macorini L. Seismic response of steel frames under repeated earthquake ground motions. Eng Struct 2004;26(13):2021–35.
[14] Bomben L, Fasan M, Amadio C. Assessment of the effect of seismic sequences on steel X-CBF for industrial buildings. Procedia Struct Integr 2023;44:99–106.
[15] Bedon C., Fasan M., Bomben L. (2024). Fattore di comportamento per telai controventati soggetti a sequenze sismiche. Technical Report (33 pages). WP12: Strutture in acciaio e composte acciaiocalcestruzzo - Contributi normativi relativi a costruzioni civili e industriali di acciaio e composte acciaio-calcestruzzo; Task 1: Edifici civili ad uso residenziale e/o uffici; UR8 Trieste (in Italian).
[16] Lolli B. Aftershocks hazard in Italy part i: estimation of time-magnitude distribution model parameters and computation of probabilities of occurrence. J Seismol 2003;7:235–57.
[17] Iervolino I, Giorgio M, Polidoro B. Sequence-based probabilistic seismic hazard analysis. Bull Seismol Soc Am 2014;104(2):1006–12.
[18] Seismosoft (2023). SeismoStruct: A Computer Program for Static and Dynamic Nonlinear Analysis of Framed Structures. Available online: https://Seismosoft.Com.
[19] EN 1993-1-1: Eurocode 3: Design of Steel Structures: Part 1-1: General Rules and Rules for Buildings, 2005.
[20] Menegotto M., Pinto P.E. (1973). Method of Analysis for Cyclically Loaded R.C. Plane Frames Including Changes in Geometry and Non-Elastic Behaviour of Elements under Combined Normal Force and Bending. Proceedings of IABSE Symposium on Resistance and Ultimate Deform ability of Structures Acted on by Well Defined Repeated Loads, 11: 15-22.
[21] Hsiao PC, Lehman DE, Roeder CW. A model to simulate special concentrically braced frames beyond brace fracture. Earthq Eng Struct Dyn 2012;42(2):183–200.
[22] Hsiao PC, Lehman DE, Roeder CW. Improved analytical model for special concentrically braced frames. J Constr Steel Res 2012;73:84–94.
[23] Hancock J, Bommer JJ, Stafford PJ. Numbers of scaled and matched accelerograms required for inelastic dynamic analyses. Earthq Eng Struct Dyn 2008;37(14):1585–607.
[24] Baltzopoulos G, Baraschino R, Iervolino I. On the number of records for structural risk estimation in PBEE. Earthq Eng Struct Dyn 2018;48(5):489–506.
[25] Kiani J, Camp C, Pezeshk S. On the number of required response history analyses. Bull Earthq Eng 2018;16:5195–226.
[26] Zentner I, Gündel M, Bonfils N. Fragility analysis methods: review of existing approaches and application. Nucl Eng Des 2017;323:245–58.
[27] Mattei S, Fasan M, Bedon C. On the use of cloud analysis for structural glass members under seismic events. Sustainability 2021;13(16):9291. https://doi.org/10.3390/su13169291.
[28] Smiroldo G, Fasasn M, Bedon C. Non-regularity damage evaluation in reinforced concrete structures via fragility curves. Vibroengineering Procedia 2023;50:28–34.
[29] Jalayer F, Ebrahimian H, Miano A, Manfredi G, Sezen H. Analytical fragility assessment using unscaled ground motion records. Earthq Eng Struct Dyn 2017;46(15):2639–63.
[30] Jalayer F, De Risi R, Manfredi G. Bayesian cloud analysis: efficient structural fragility assessment using linear regression. Bull Earthq Eng 2015;13:1183–203.
[31] Luco N, Bazzurro P. Does amplitude scaling of ground motion records result in biased nonlinear structural drift responses. Earthq Eng Struct Dyn 2007;36(13):1813–35.
[32] Zacharenaki A, Fragiadakis M, Assimaki D, Papadrakakis M. Bias assessment in incremental dynamic analysis due to record scaling. Soil Dyn Earthq Eng 2014;67:158–68.
[33] Jalayer F, Cornell CA. Alternative non-linear demand estimation methods for probability-based seismic assessments. Earthq Eng Struct Dyn 2009;38(8):951–72.
[34] Luzi L., Lanzano G., Felicetta C., D'Amico M.C., Russo E., Sgobba S., Pacor, F., ORFEUS Working Group 5 (2020). Engineering Strong Motion Database (ESM), Version 2.0, Istituto Nazionale di Geofisica e Vulcanologia (INGV), https://doi.org/10.13127/ESM.2.
[35] National Research Institute for Earth Science and Disaster Resilience. NIED K-NET and KiK-net, https://www.doi.org/10.17598/NIED.0004. Available online: https://www.kyoshin.bosai.go.jp/.

[36] Fasan M. (2021). Develop Fragility Curves as a Function of Intensity for Full SRA in Intensity Domain. Technical Report Ref: SIGMA2-2021-D6-087 (45 pages). Available online: https://www.sigma-2.net/medias/files/sigma2-2021-d6-087-develop-fragility-curves-as-a-function-of-macroseismic-intensity-rv1-signedrev.pdf.
[37] Boore DM. Orientation-independent measures of ground motion. Bull Seismol Soc Am 2006;96(4A):1502–11.
[38] Iervolino I. Assessing uncertainty in estimation of seismic response for PBEE. Earthq Eng Struct Dyn 2017;46(10):1711–23.
[39] Pitilakis K, Crowley E, Crowley E. SYNER-G: Typology Definition and Fragility Functions for Physical Elements at Seismic Risk – Buildings, Lifelines. Transportation Networks and Critical Facilities. Springer Nature; 2014. p. 437. ISBN: 9789400778719.
[40] Bakalis K, Vamvatsikos D. Seismic fragility functions via nonlinear response history analysis. J Struct Eng 2018;144(10). https://doi.org/10.1061/(ASCE)ST.1943-541X.000214.
[41] Silva V, Akkar S, Baker J, Bazzurro P, Castro JM, Crowley H, et al. Current challenges and future trends in analytical fragility and vulnerability modeling. Earthq Spectra 2019;35(4). https://doi.org/10.1193/042418EQS101O.